Fluctuation-dissipation bounds in time-dependently driven conductors

Editors' Suggestion

Fluctuation-dissipation bounds in time-dependently driven conductors

Ludovico Tesser,[1] José Balduque,[2,3] and Janine Splettstoesser[1]
[1]*Department of Microtechnology and Nanoscience (MC2), Chalmers University of Technology, S-412 96 Göteborg, Sweden*
[2]*Departamento de Física Teórica de la Materia Condensada, Universidad Autónoma de Madrid, 28049 Madrid, Spain*
[3]*Condensed Matter Physics Center (IFIMAC), Universidad Autónoma de Madrid, 28049 Madrid, Spain*

(Received 9 September 2025; revised 22 January 2026; accepted 3 February 2026; published 2 March 2026)

We analyze the noise in a multiterminal multichannel conductor under arbitrary time-dependent driving and subject to—possibly large—static potential and temperature biases. We show that the full out-of-equilibrium zero-frequency noise is constrained by a fluctuation-dissipation bound. It consists of an upper bound expressed in terms of weighted current components of the separate Floquet bands arising from the time-dependent driving. In the limit of large static temperature bias, it has an intuitive interpretation in terms of the dissipated powers due to the static potential bias and due to the time-dependent driving. Furthermore, we show the existence of a second bound that relies on the specific shape of the electron distribution resulting from the driving, which can even be tighter than the fluctuation-dissipation bound in some parameter regimes. We show the implications of our bounds at the simple but experimentally relevant example of a two-terminal conductor in the presence of an ac bias.

DOI: 10.1103/q757-fw25

I. INTRODUCTION

Precision plays an important role in small-scale systems, where the magnitude of fluctuations can be significant with respect to the desired average observable. For example, thermoelectric nanoscale conductors can serve as engines [1–4], transforming tiny amounts of heat into electrical power at a few-particle level or vice versa by using electrical power as a resource for cooling [5]. In quantum transport, driven nanoscale conductors furthermore serve as precise current sources [6–8]. Hence, knowledge about how the power and current fluctuations behave is crucial [9,10]. It is of particular interest to understand how the fluctuations are related to the desired average output. At equilibrium or close to equilibrium, a relation between noise and average response is provided by fluctuation-dissipation theorems [11–14]. But even out of equilibrium, similar relations have been found for systems with a weak tunnel coupling and subject to a voltage bias [15–17] or to time-dependent driving [18,19]. Also, far from equilibrium, relations like the fluctuation-dissipation theorem can be established under stalling conditions [20,21] or using cumulant expansions of the full-counting statistics [22–24].

When releasing the constraints set by the specific out-of-equilibrium conditions, fluctuation-dissipation theorems are not available any longer. Nonetheless, important information on the minimum amount of fluctuations that occur in a process have been formulated in terms of fluctuation bounds [25]. These bounds have different purposes and origins: the so-called thermodynamic uncertainty relation [26,27] constrains the precision by the entropy production; the kinetic uncertainty relation constrains the precision in terms of the activity of a process [28]. Both of these bounds were originally developed for classical processes. The challenge of treating coherent quantum transport in conductors that are possibly strongly coupled to the contacts has been tackled in Refs. [29–33], and also bounds on the full statistics have very recently been addressed [34]. Furthermore, for this coherent, strong coupling situation, a fluctuation-dissipation bound has been developed, constraining the amount of nonequilibrium noise by the nonequilibrium conditions (temperature and voltage bias) and by the desired current flow resulting from it [35] (see also a recent extension to energy transport [36]). However, noise bounds for coherent quantum transport

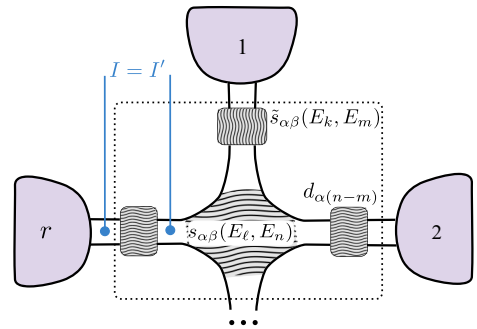

FIG. 1. Sketch of the multiterminal setup with contacts $\alpha = 1, .., r$. Time-dependent driving is applied in the leads and in the central region (patterned). Measurements of the time-averaged current and of the zero-frequency noise, when performed before or after the driven lead region (blue spots), yield the same result.

under time-dependent driving have until now been limited to thermodynamic bounds in terms of entropy production and to linear response [37] or slow driving [38]. Also, recently developed more generally valid bounds on the transition rates provide simple statements for the noise only in the regime of weak tunnel coupling [39]. Understanding limits on noise in the presence of arbitrary time-dependent driving *and* temperature bias, is, however, important for the precision of cyclically operating heat engines as well as for time-dependently driven conductors in which accidental temperature differences arise due to the operation of the device, where they can strongly impact the precision.

In this paper, we address this shortage and extend the nonequilibrium fluctuation-dissipation bound of Ref. [35], which is valid in the stationary regime, to systems with generic time-dependent driving on top of static out-of-equilibrium conditions set by temperature and potential differences. This includes both driving of the central conductor, for example, by a modulation of gate voltages, as well as time-dependent driving applied to the contacts, such as time-dependent bias voltages or even time-dependent temperatures [40] which can be modeled by an effective time-dependent Hamiltonian [41]. We establish a bound on the noise, more precisely on the zero-frequency charge-current autocorrelators (or integrated current-current correlator), by comparing situations with and without voltage and temperature biases in the presence of the driving. We show that the nonequilibrium fluctuations are bounded by a weighted sum over spectral current components. This fluctuation-dissipation bound for time-dependent systems, in the presence of considerable temperature differences, equals the power provided by or absorbed by the drive and the power dissipated due to the stationary nonequilibrium conditions. We furthermore develop an additional, so-called intersection bound, which is often tighter than the fluctuation-dissipation bound but is expressed in terms of the full electronic distribution functions modified by the time-dependent driving.

To set up these bounds, we use scattering theory, thereby fully treating quantum coherences and strong coupling, which is in contrast to typical stochastic approaches [14,25]. This comes at the cost of treating Coulomb interactions only up to the mean-field level. Note, however, that the fact that our bounds hold for scattering matrices for an arbitrary time-dependent driving has an important implication: our theory indeed fully includes the treatment of possible mean-field screening potentials due to the time-dependent driving that affect currents and noise [42–46] and the developed bounds are valid even if the effect of the screening potentials on the scattering matrix is not explicitly known.

The remainder of this paper is organized as follows. We introduce the model for the driven multiterminal, multichannel conductor in Sec. II A. In Sec. II, we also show how relevant observables, namely, charge currents and charge-current noise as well as energy and heat currents revealing the role of the dissipated or provided power, are obtained from Floquet scattering theory for time-dependently driven conductors. We then derive the out-of-equilibrium dissipation bound for time-dependently driven systems in Sec. III A and show its intuitive interpretation in the limit of large temperature bias in Sec. III B. The alternative intersection bound in terms of effective distribution functions is presented in Sec. III C. In Sec. IV, these bounds are demonstrated at the example of an ac-biased two-terminal conductor in the presence of a temperature difference. Detailed derivations are provided in the Appendixes.

II. MODEL AND APPROACH

A. Multiterminal setup

We study a multiterminal, multichannel conductor subject to stationary out-of-equilibrium conditions due to different temperatures and electrochemical potentials in the contacts and subject to arbitrary time-dependent driving. We describe the setup, sketched in Fig. 1, by Floquet scattering theory [47]; see also Refs. [48,49].

The contacts of this multiterminal setup are labeled by Greek letters $\alpha, \beta, \gamma = 1, ..., r$. Each contact α is described by a macroscopic distribution function characterized by Fermi functions with a given temperature $T_\alpha = \bar{T} + \Delta T_\alpha$ compared to an equilibrium temperature $\bar{T}$ and electrochemical potential $\mu_\alpha = \bar{\mu} + qV_\alpha^{\mathrm{dc}}$ compared to an equilibrium potential $\bar{\mu}$. Here we introduced the charge of the quasiparticle excitations q, which is typically going to be the electron charge. Excitations leaving the contact and impinging on the scattering region via channel $n = 1, ..., N_\alpha$ are characterized by creation and annihilation operators, $\hat{a}^\dagger_{\alpha n}(E)$ and $\hat{a}_{\alpha n}(E)$, fulfilling

$$\langle \hat{a}^\dagger_{\alpha n}(E)\hat{a}_{\beta m}(E')\rangle = \delta_{\alpha\beta}\delta_{nm}\delta(E-E')f_\alpha(E), \tag{1}$$

with channel index n counting the N_α channels in contact α. Here, $f_\alpha(E)$ denotes the Fermi function and we will later use the definition $f^-_\alpha(E) := 1 - f_\alpha(E)$. These excitations get scattered in the conductor while picking up an integer amount of Floquet quanta due to the time-dependent driving. By contrast, the excitations leaving the scatterer and impinging on the contacts are characterized by creation and annihilation operators, $\hat{b}^\dagger_{\alpha n}(E)$ and $\hat{b}_{\alpha n}(E)$, fulfilling

$$\langle \hat{b}^\dagger_{\alpha n}(E)\hat{b}_{\alpha n}(E')\rangle = \tilde{s}^*_{\alpha n,\beta m}(E,E_k)\tilde{s}_{\alpha n,\beta m}(E',E'_\ell) \times f_\beta(E_k)\delta(E-E'-(\ell-k)\hbar\Omega), \tag{2}$$

where the sum over additional indices appearing on the right-hand side is from here on always implicit if not otherwise indicated. Here we have introduced the Floquet scattering matrix elements $\tilde{s}_{\alpha n,\beta m}(E,E_k)$, which provide the amplitude for an excitation incoming from channel m in contact β at energy $E_k = E + k\hbar\Omega$ to be scattered into channel n of contact α while exchanging $-k$ Floquet quanta $\hbar\Omega$. This exchange of Floquet quanta in the scattering process arises from the time-dependent driving, which we here assume to result from the driving of any set of parameters $\{X(t)\}$ that can be decomposed in a Fourier series with frequency Ω, namely, $X(t) = \sum_n e^{-in\Omega t}X_n$. The scattering matrix fulfills a unitarity condition [47]; see also Appendix A.

To model different types of experimentally relevant settings, it can be useful to decompose the scattering matrix into parts describing the backscattering free evolution due to driving in the lead regions and scattering between different contacts under the influence of driving in the central region,

see Fig. 1, as

$$\tilde{s}_{\alpha n,\beta m}(E,E_k) \equiv d_{\alpha\ell} s_{\alpha n,\beta m}(E_{-\ell},E_{k+p}) c_{\beta p}. \tag{3}$$

Here we introduce the Floquet scattering matrix of the central region only, $s_{\alpha n,\beta m}(E_{-\ell},E_{k+p})$, as well as the Floquet coefficients due to the ac driving in the leads, $d_{\alpha\ell}$, $c_{\beta p}$ which are defined as

$$d_{\alpha\ell} = \int_0^{\mathcal{T}} \frac{dt}{\mathcal{T}} e^{-i\phi_\alpha(t)} e^{i\ell\Omega t}, \tag{4a}$$

$$\phi_\alpha(t) = \frac{q}{\hbar}\int_0^t dt' V_\alpha^{\rm ac}(t'), \tag{4b}$$

$$V_\alpha^{\rm ac}(t) = \sum_n V_{\alpha n} e^{-in\Omega t}, \tag{4c}$$

and equivalently for $c_{\beta p}$ for a generally different ac-driving potential. Here $\mathcal{T} = 2\pi/\Omega$ is the period of the drive. Note that introducing the lead driving with potential $V_\alpha^{\rm ac}(t)$ is also a convenient way to model the ac part of a time-dependent bias voltage in a contact [47]. The scattering matrix $s_{\alpha n,\beta m}(E_{-\ell},E_{k+p})$ can, in principle, contain any type of effect due to time-dependent driving, including screening-induced time-dependent potentials.

B. Currents and fluctuations

We are interested in the time-averaged charge current and its zero-frequency noise. To evaluate these observables, we start from the time-dependent current operator:

$$\hat{I}_\alpha(t) = \frac{q}{h}\int dE\, dE'\, e^{i(E-E')t/\hbar} \times [\hat{b}^\dagger_{\alpha n}(E)\hat{b}_{\alpha n}(E') - \hat{a}^\dagger_{\alpha n}(E)\hat{a}_{\alpha n}(E')]. \tag{5}$$

Evaluating the expectation value, $I_\alpha(t) = \langle \hat{I}_\alpha(t)\rangle$, and its time average, $I_\alpha = \int_0^{\mathcal{T}} I_\alpha(t)dt/\mathcal{T}$, namely, the dc component of the current, we find

$$I_\alpha = q\int \frac{dE}{h}(\mathrm{Tr}\{\tilde{t}^\dagger_{\alpha\beta}(E,E_k)\tilde{t}_{\alpha\beta}(E,E_k)\} \times f_\beta(E_k) - N_\alpha f_\alpha(E)). \tag{6}$$

Here we have introduced submatrices $\tilde{t}_{\alpha\beta}(E,E_k)$ of the scattering matrix with elements $[\tilde{t}_{\alpha\beta}(E,E_k)]_{nm} = \tilde{s}_{\alpha n,\beta m}(E,E_k)$ to keep the notation compact; the trace in Eq. (6) is hence taken over all channels $n = 1,\ldots,N_\alpha$, while additional (implicit) sums are performed over indices β and k. Note that in the leads no backscattering is induced due to the driving, as characterized by the Floquet coefficients $d_{\alpha\ell}$, $c_{\beta p}$. Therefore, a measurement of the time-averaged current (as well as of the zero-frequency charge-current noise) before or after the driven lead region, indicated by blue spots in Fig. 1, yields identical results due to current conservation. Starting from the current, we calculate the linear conductances which for $\alpha \neq \beta$ are defined as

$$G_{\alpha\beta} := \left.\frac{\partial I_\alpha}{\partial V_\beta}\right|_{\{\mu_\beta=\mu_\alpha, T_\beta=T_\alpha\}}. \tag{7}$$

In terms of scattering matrices, they take the explicit form

$$G_{\alpha\beta} = \frac{q^2}{h}\int dE\ \mathrm{Tr}\{\tilde{t}^\dagger_{\alpha\beta}(E_k,E)\tilde{t}_{\alpha\beta}(E_k,E)\} \times \frac{1}{k_{\rm B}T_\alpha} f_\alpha(E) f_\alpha^-(E). \tag{8}$$

Note that this is the linear conductance in the presence of full time-dependent driving.

In analogy to the charge current, the energy current flowing into contact α in the driven system is given by [47,50]

$$I^E_\alpha = \int dE\ \frac{E}{h}\mathrm{Tr}\{\tilde{t}^\dagger_{\alpha\beta}(E,E_k)\tilde{t}_{\alpha\beta}(E,E_k)\} \times (f_\beta(E_k) - f_\alpha(E)). \tag{9}$$

The energy current is the starting point to calculate heat currents and dissipated power, see Sec. III B and Appendix B, which plays an important role in the fluctuation-dissipation bound we develop.

Indeed, the quantity of central interest here is the noise. Concretely, we consider the zero-frequency auto-correlations in one of the contacts. In the following Sec. III A, we always assume that the noise is measured in the hottest contact. Nonetheless, we here start from the definition for the zero-frequency noise of $\hat{I}_\alpha$ in any contact α,

$$\mathcal{S}_{\alpha\alpha} := \int_0^{\mathcal{T}} \frac{dt}{\mathcal{T}} \int d\tau \langle \delta\hat{I}_\alpha(t+\tau)\delta\hat{I}_\alpha(t)\rangle, \tag{10}$$

with $\delta\hat{I}_\alpha(t) := \hat{I}_\alpha(t) - I_\alpha$. Using the definition of the current operator, given in Eq. (5), and plugging in the full Floquet scattering matrix (2), we find

$$\mathcal{S}_{\alpha\alpha} = \frac{q^2}{h}\int dE f_\beta(E_{k_1}) f^-_\gamma(E_{k_2}) \times \mathrm{Tr}\{(\tilde{t}^\dagger_{\alpha\beta}(E,E_{k_2})\tilde{t}_{\alpha\gamma}(E,E_{k_2}) - \delta_{\alpha\beta}\delta_{\alpha\gamma}\delta_{k_1k_2}\delta_{k_1\ell_2}\delta_{k_2\ell_1}) \times (\tilde{t}^\dagger_{\alpha\gamma}(E_{k_2-\ell_1},E_{k_2})\tilde{t}_{\alpha\beta}(E_{k_1-\ell_2},E_{k_1}) - \delta_{\alpha\beta}\delta_{\alpha\gamma}\delta_{k_1k_2})\}. \tag{11}$$

We recall that all additional (Floquet and contact) indices occurring on the right-hand side are summed over. We evaluate this expression starting from terms that are of zeroth, second, and fourth order in the scattering matrices, $\mathcal{S}_{\alpha\alpha} = \mathcal{S}^{(0)}_{\alpha\alpha} + \mathcal{S}^{(2)}_{\alpha\alpha} + \mathcal{S}^{(4)}_{\alpha\alpha}$ with

$$\mathcal{S}^{(0)}_{\alpha\alpha} := \frac{q^2}{h}\int dE f_\alpha(E) f^-_\alpha(E) N_\alpha\ , \tag{12a}$$

$$\mathcal{S}^{(2)}_{\alpha\alpha} := -2\frac{q^2}{h}\int dE \mathrm{Tr}\{\tilde{t}^\dagger_{\alpha\alpha}(E,E_k)\tilde{t}_{\alpha\alpha}(E,E_k)\} \times f_\alpha(E_k) f^-_\alpha(E_k), \tag{12b}$$

as well as

$$S^{(4)}_{\alpha\alpha} := \frac{q^2}{h}\int dE \mathrm{Tr}\{\tilde{t}_{\alpha\beta}(E_\ell,E_k)\tilde{t}^\dagger_{\alpha\beta}(E,E_k) \times \tilde{t}_{\alpha\gamma}(E,E_p)\tilde{t}^\dagger_{\alpha\gamma}(E_\ell,E_p)\} f_\beta(E_k) f^-_\gamma(E_p). \tag{12c}$$

Below we use these compact expressions to derive the out-of-equilibrium fluctuation-dissipation bound for time-dependently driven systems, as well as an alternative bound we refer to as intersection bound, in Sec. III A and Appendix C.

III. FLUCTUATION-DISSIPATION BOUNDS

In the following, we derive general bounds on the noise, valid for any realization of the scattering matrix, any stationary bias, and any type of periodic time-dependent driving. We will express these bounds in terms of an excess noise, namely, comparing the noise of the full nonequilibrium system to an expression containing linear conductances; in the absence of time-dependent driving, this expression equals the thermal noise.

A. Fluctuation-dissipation bound for time-dependently driven systems

The derivation of the fluctuation-dissipation bound for time-dependently driven systems consists of three major steps starting from the full noise expression from scattering theory, Eq. (11). We first split off a contribution related to the linear conductance. Then we demonstrate that the noise term in fourth order in the scattering matrices is bounded and identify the part that always reduces the noise. Finally, we compare the relative magnitude of the distribution functions of the different contacts in energy intervals separated by the crossing points between these distribution functions.

Now, as a first step toward the derivation of the fluctuation-dissipation bound in the presence of time-dependent driving, we establish how the noise under full nonequilibrium conditions, namely, in the presence of voltage and temperature biases *and* in the presence of an arbitrary driving, relates to the linear conductances found when all static electrochemical potentials and temperatures are the same. We therefore first rewrite the term $\mathcal{S}^{(2)}_{\alpha\alpha}$ given in Eq. (12b) in terms of a contribution that contains the linear conductance of Eq. (8),

$$\mathcal{S}^{(2)}_{\alpha\alpha} = 2k_{\mathrm{B}}T_\alpha \sum_{\beta\neq\alpha} G_{\alpha\beta} - 2\frac{q^2}{h}\int dE N_\alpha f_\alpha(E) f^-_\alpha(E), \tag{13}$$

together with an additional term in the second row that will partially cancel with $\mathcal{S}^{(0)}_{\alpha\alpha}$, see Eq. (12a). Highlighting the linear conductance in the presence of driving has the advantage that it provides the opportunity for connections to the thermal noise, since it appears in the equilibrium fluctuation-dissipation theorem.

Furthermore, rewriting the remaining term that is quartic in the scattering amplitudes, $\mathcal{S}^{(4)}_{\alpha\alpha}$ given in (12c), and using the Cauchy-Schwarz inequality as explained in Appendix C, we find a constraint on the full noise with respect to the linear conductances:

$$\begin{aligned}\mathcal{S}_{\alpha\alpha} - 2k_{\mathrm{B}}T_\alpha \sum_{\beta\neq\alpha} G_{\alpha\beta} \\ \leqslant \frac{q^2}{h}\int dE \mathrm{Tr}\{\tilde{t}_{\alpha\beta}(E,E_k)\tilde{t}^\dagger_{\alpha\beta}(E,E_k)\} \\ \times (1-2f_\alpha(E))(f_\beta(E_k)-f_\alpha(E)).\end{aligned} \tag{14}$$

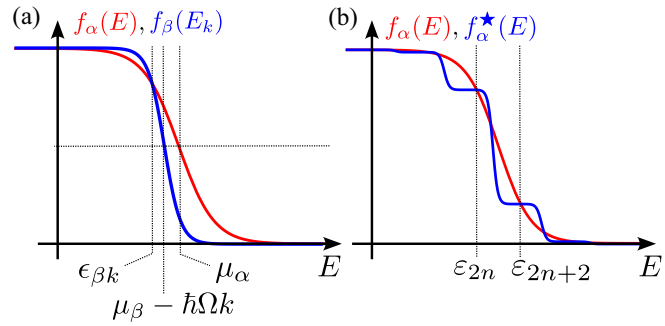

FIG. 2. (a) Crossing of the Fermi function characterizing the hot contact with the Fermi function characterizing the cold contact, shifted by k Floquet quanta. (b) Crossing of the occupation of the hot contact with the occupation stemming from the other contact(s) modified by the driving (here for an example with ac-driving in the contacts and full transmission $D = 1$).

The expression on the right-hand side is similar to the current, apart from the factor $1 - 2f_\alpha(E)$ in the integrand.

Finally, since we know that $1 - 2f_\alpha(E)$ is an increasing function in energy, we can bound the right-hand side of the inequality (14) by opportunely replacing $1 - 2f_\alpha(E)$ with a convenient constant value, which can then be taken out of the energy integral. To make this replacement, we now choose contact α, in which the current is measured, to be the hottest one, i.e., $T_\alpha > T_\beta$ for all $\beta \neq \alpha$. We then identify the energy at which the Fermi functions $f_\beta(E_k)$, $f_\alpha(E)$ cross for each value of k. This crossing energy, indicated in Fig. 2(a), is

$$\epsilon_{\beta k} := \frac{T_\alpha(\mu_\beta - \hbar\Omega k) - T_\beta\mu_\alpha}{T_\alpha - T_\beta}. \tag{15}$$

At energies smaller than the crossing energy, we have $f_\beta(E_k) - f_\alpha(E) > 0$ as well as $1 - 2f_\alpha(E) < 1 - 2f_\alpha(\epsilon_{\beta k})$, while at energies larger than the crossing energy, we have $f_\beta(E_k) - f_\alpha(E) < 0$ as well as $1 - 2f_\alpha(E) > 1 - 2f_\alpha(\epsilon_{\beta k})$.

We can therefore write the following constraint for the noise:

$$\mathcal{S}_{\alpha\alpha} - 2k_{\mathrm{B}}T_\alpha \sum_{\beta\neq\alpha} G_{\alpha\beta} \leqslant q\sum_{\beta,k}(1-2f_\alpha(\epsilon_{\beta k}))I_{\alpha\beta,k} \tag{16}$$

in terms of the contact-resolved current components for each Floquet band:

$$\begin{aligned}I_{\alpha\beta,k} := q\int \frac{dE}{h}\mathrm{Tr}\{\tilde{t}_{\alpha\beta}(E,E_k)\tilde{t}^\dagger_{\alpha\beta}(E,E_k)\} \\ \times (f_\beta(E_k) - f_\alpha(E)).\end{aligned} \tag{17}$$

The constraint (16) is the central result of this paper. We refer to it as the fluctuation-dissipation bound for time-dependent driving (t-FDB). It shows that the full nonequilibrium zero-frequency noise compared to the linear response function in the absence of static biases is bounded by a weighted sum of spectral currents. We emphasize that this bound holds for any scattering matrix as long as the driving can be decomposed in a Fourier series; this means in particular that the bound also holds if screening effects induced by the driving modify the scattering landscape. In the absence of driving, it reduces to the stationary FDB presented in Ref. [35]. Using the explicit expression for the crossing energy in Eq. (15), the t-FDB (16)

can be rewritten as

$$\mathcal{S}_{\alpha\alpha} - 2k_{\mathrm{B}}T_\alpha \sum_{\beta\neq\alpha} G_{\alpha\beta} \leqslant -q \sum_{\beta,k} \tanh\left\{\frac{\mu_\alpha - \mu_\beta + \hbar\Omega k}{2k_{\mathrm{B}}(T_\alpha - T_\beta)}\right\} I_{\alpha\beta,k}. \quad (18)$$

In the following, we provide an intuitive interpretation of this bound, which is particularly relevant in the limit of large temperatures biases.

B. Limit of large temperature bias

Large temperature biases are of special interest for, e.g., heat engines. At the same time, typical extensions of the equilibrium fluctuation-dissipation theorem fail at large temperature differences. When the nonequilibrium situation is established by large temperature biases, $\Delta T_{\alpha\beta} \equiv T_\alpha - T_\beta$ compared to the sum of potential biases $\Delta\mu_{\alpha\beta} \equiv \mu_\alpha - \mu_\beta$ and a relevant number of Floquet quanta, namely, for $k_{\mathrm{B}}\Delta T_{\alpha\beta} \gg \Delta\mu_{\alpha\beta} + \hbar\Omega k$, the weighting factor of the current components in Eq. (18) can be expanded. Importantly, this situation cannot be covered by any close-to-equilibrium FDT [11–13] or by extensions to finite bias voltage [15,16] or driving [18,19] where an overall equilibrium temperature is assumed. By studying this limit, we thus complement previous results for the important case where a quantum conductor is subject not only to driving but also to a large temperature differences. We find in this limit

$$\mathcal{S}_{\alpha\alpha} - 2k_{\mathrm{B}}T_\alpha \sum_{\beta\neq\alpha} G_{\alpha\beta} \leqslant -\frac{q}{2k_{\mathrm{B}}}\left(\sum_{\beta,k} \frac{\Delta\mu_{\alpha\beta}}{\Delta T_{\alpha\beta}} I_{\alpha\beta,k} + \sum_{\beta,k} \hbar\Omega k \frac{I_{\alpha\beta,k}}{\Delta T_{\alpha\beta}}\right). \quad (19)$$

These two contributions are related to the power due to the potential bias and due to the driving, which, as shown in Appendix B, fulfill

$$\sum_{\alpha,\beta,k} \Delta\mu_{\alpha\beta} I_{\alpha\beta,k} = 2q\bar{\mathcal{P}}^{\mathrm{pot}}, \quad (20)$$

$$\sum_{\alpha,\beta,k} \hbar\Omega k I_{\alpha\beta,k} = 2q\bar{\mathcal{P}}^{\mathrm{driv}}. \quad (21)$$

Here we define the symmetrized power $\bar{\mathcal{P}}^{\mathrm{x}} = \frac{1}{2}(\mathcal{P}^{\mathrm{x}} + \mathcal{P}^{\mathrm{x,tr}})$ as the average between the power in the actual and in the time-reversed (tr) system. The expressions in (19) hence correspond to the lead-resolved contributions $\bar{\mathcal{P}}^{\mathrm{x}}_{\alpha\beta}$ to these symmetrized powers, $\bar{\mathcal{P}}^{\mathrm{x}} = \sum_{\alpha\beta} \bar{\mathcal{P}}^{\mathrm{x}}_{\alpha\beta}$. With this, we write the bound in the limit of large temperature biases as

$$\mathcal{S}_{\alpha\alpha} - 2k_{\mathrm{B}}T_\alpha \sum_{\beta\neq\alpha} G_{\alpha\beta} \leqslant -q^2 \sum_{\beta} \frac{\left(\bar{\mathcal{P}}^{\mathrm{pot}}_{\alpha\beta} + \bar{\mathcal{P}}^{\mathrm{driv}}_{\alpha\beta}\right)}{k_{\mathrm{B}}\Delta T_{\alpha\beta}}. \quad (22)$$

In a system where time-reversal symmetry is not broken, the symmetrized functions $\bar{\mathcal{P}}^{\mathrm{x}}$ equal the powers $\mathcal{P}^{\mathrm{x}} = \mathcal{P}^{\mathrm{x,tr}}$. This is, for example, the case for the two-terminal system discussed in Sec. IV, where the driving is applied only to one of the leads and not to the energy-dependent central scattering region connecting different contacts. The bound (22) hence shows that it depends on whether the power is dissipated ($\mathcal{P} < 0$) or produced ($\mathcal{P} > 0$) to which extent the out-of-equilibrium noise is allowed to be larger or constrained to be smaller than the equilibrium-like noise in the absence of temperature and voltage biases. This interpretation of the noise bounds in terms of dissipated or generated power is an asset of the t-FDB compared to the intersection bound presented in the next Sec. III C (which instead turns out to often be a tighter bound). In the absence of driving, the bound (22) reproduces the result obtained in Ref. [35], where power is dissipated due to an applied stationary bias voltage or produced due to a temperature bias in coherent conductors with thermoelectric (energy-filtering) properties.

C. Intersection bound for nonthermal distributions

The time-dependent driving applied to the leads or to the central conductor as well as the mixing of occupations from different baths result in modified distributions entering a given contact. Such modified distributions in systems where thermalization is hindered are also referred to as athermal [51,52] or nonthermal [53–55] distributions. Another way of setting up a noise bound, complementary to (18), is by identifying the crossings of such nonthermal distribution functions. Therefore, we start from relation (14) and define the modified distribution function

$$f^{\bigstar}_\alpha(E) = \frac{1}{N_\alpha}\mathrm{Tr}\{\tilde{t}_{\alpha\beta}(E,E_k)\tilde{t}^\dagger_{\alpha\beta}(E,E_k)\}f_\beta(E_k). \quad (23)$$

This modified distribution function can be either larger or smaller than the hot distribution $f_\alpha(E)$ in different energy intervals. This means that sign changes in the difference between them occur at given energies ε_n, with $n = 1, ..., M$. The M crossing energies between the occupation functions, see Fig. 2(b) for an example, are found from $g(\varepsilon) \equiv f^{\bigstar}_\alpha(\varepsilon) - f_\alpha(\varepsilon) = 0$ with $g'(\varepsilon) \neq 0$. Note that, since f_α is the hottest distribution, there is a (low) energy below which $f_\alpha(E) < f^{\bigstar}_\alpha(E)$ and a (high) energy above which $f_\alpha(E) > f^{\bigstar}_\alpha(E)$. This guarantees the number of crossing points M between $f_\alpha(E)$ and $f^{\bigstar}_\alpha(E)$ to be odd. With this, we find the bound

$$\mathcal{S}_{\alpha\alpha} - 2k_{\mathrm{B}}T_\alpha \sum_{\beta\neq\alpha} G_{\alpha\beta} \leqslant q^2 \sum_{n=0}^{\frac{M-1}{2}} (1 - 2f_\alpha(\varepsilon_{2n+1})) \times N_\alpha \int_{\varepsilon_{2n}}^{\varepsilon_{2n+2}} \frac{dE}{h}(f^{\bigstar}_\alpha(E) - f_\alpha(E)), \quad (24)$$

where we set the convention $\varepsilon_0 = -\infty$ and $\varepsilon_{M+1} = \infty$. The second line of (24) corresponds to the current contribution from the energy window $[\varepsilon_{2n}, \varepsilon_{2n+2}]$. We refer to the constraint (24) as the intersection bound. This bound can be expected to often be tighter than the t-FDB (16), since the intersection bound relies on estimates adapted separately for energy intervals limited by the identified crossing points. This comes at the cost of providing less physical insight than the t-FDB, since the position of the crossings is not generally known, but needs to be evaluated for each specific nonthermal distribution $f^{\bigstar}_\alpha(E)$. Therefore, also a direct connection of the bound to other transport quantities such as the total dissipated power, in analogy to (22), cannot be straightforwardly established.

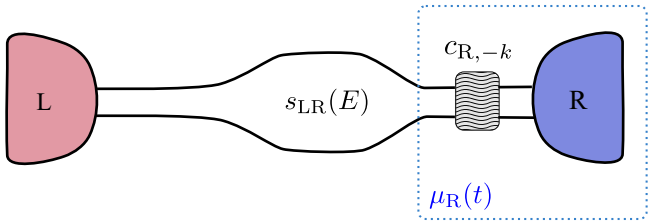

FIG. 3. Sketch of the two-terminal system with a nondriven but possibly energy-dependent central scattering region. Time-dependent driving is applied to the right contact, modeled via Floquet coefficients in the right lead region. Contact L at which the current and noise are measured is hotter than contact R (before the driven region, indicated in blue).

Note that intersection bounds of this type can be found in different shapes, depending on the definition of the effective distribution function, namely, depending on which part of the full scattering matrix is incorporated into the modified distribution function; see also Appendix D. We anticipate that these types of intersection bounds could also be extended to arbitrary nonthermal distributions, which are not necessarily generated by a time-dependent driving, in contact with one thermal hotter one. Here, hotter means that the distribution is smaller than the nonthermal one for $E \to -\infty$ and larger than the nonthermal one for $E \to \infty$.

IV. TWO-TERMINAL CONDUCTOR DRIVEN BY AN AC BIAS VOLTAGE

To demonstrate the characteristics and predictiveness of the developed noise bounds, we finally present a simple example of a two-terminal single-channel system in which only one of the contacts is driven by a time-dependent voltage; see Fig. 3. Specifically, we choose L to be the contact where the current and noise are measured, with $T_{\mathrm{L}} > T_{\mathrm{R}} \equiv T$ and $\mu_{\mathrm{L}} = \bar{\mu}$, while R is subject to a time-dependent bias voltage, such that $\mu_{\mathrm{R}}(t) = \bar{\mu} + qV_{\mathrm{R}}^{\mathrm{dc}} + qV_{\mathrm{R}}^{\mathrm{ac}}(t)$. The constant parts of the potentials enter the Fermi functions of the two contacts. The scattering matrix of this system is given by

$$\tilde{s}_{\mathrm{LR}}(E, E_k) = s_{\mathrm{LR}}(E)c_{-k}, \quad \tilde{s}_{\mathrm{LL}}(E, E_k) = s_{\mathrm{LL}}(E)\delta_{k0}. \tag{25}$$

Here, the Floquet coefficients used to model the ac part of the potential in R are given by c_{-k}. The scattering matrix $s_{\mathrm{LR}}(E)$ of the central region depends on one energy only, since the driving is applied to the contacts—or, equivalently, the leads—only. We define the transmission probability of the central region as $D(E) = |s_{\mathrm{LR}}(E)|^2$. Below, we choose two examples, namely, a transmission probability $D(E) = D_0$ of the central conductor that is energy independent in the energy interval relevant for transport or an energy filter with a transmission of boxcar shape.

In the simple two-terminal system subject to an ac voltage bias, the full noise is found to be [56]

$$\begin{aligned}\mathcal{S}_{\mathrm{LL}} = \frac{q^2}{h}\int dE [&D(E)^2 f_{\mathrm{L}}(E) f_{\mathrm{L}}^{-}(E) \\ &+ D(E)D(E_\ell)c_{l-k}c^*_{-k}c_{l-p}c^*_{-p} f_R(E_k) f_{\mathrm{R}}^{-}(E_p) \\ &+ D(E)(1-D(E))(f_{\mathrm{L}}(E)\tilde{f}_{\mathrm{R}}^{-}(E_k) + f_{\mathrm{L}}^{-}(E)\tilde{f}_{\mathrm{R}}(E_k))],\end{aligned} \tag{26}$$

where the first two lines are the so-called interference contributions to the noise, which are equal to the thermal noise in the absence of driving, and the last line is the so-called transport contribution to the noise. Here, we have defined

$$\tilde{f}_{\mathrm{R}}(E) := \sum_k |c_{-k}|^2 f_{\mathrm{R}}(E_k). \tag{27}$$

As a result of the fact that the driving is directly applied to the lead only, the linear conductance G appearing on the left-hand sides of the bounds, Eqs. (16) and (24), is the same for the driven and for the static case:

$$G \equiv G_{\mathrm{LR}} = \frac{q^2}{hk_{\mathrm{B}}T_{\mathrm{L}}}\int dE\, D(E) f_{\mathrm{L}}(E) f_{\mathrm{L}}^{-}(E). \tag{28}$$

It is hence simply proportional to the thermal noise of contact L. Therefore, the excess noise on the left-hand side of the bounds indeed always represents the difference between the full nonequilibrium noise and the equilibrium noise as given by the fluctuation-dissipation theorem.

The current components of Eq. (17) are given by

$$I_{\mathrm{LR,k}} = q\int \frac{dE}{h} D(E)|c_{-k}|^2 (f_{\mathrm{R}}(E_k) - f_{\mathrm{L}}(E)). \tag{29}$$

Starting from this expression, we calculate the dissipated powers, which enter the t-FDB (16) in the limit of large temperature bias:

$$2\mathcal{P}_{\mathrm{L}}^{\mathrm{pot}} = -qV_{\mathrm{R}}^{\mathrm{dc}}\int \frac{dE}{h} D(E)|c_{-k}|^2 (f_{\mathrm{R}}(E_k) - f_{\mathrm{L}}(E)), \tag{30}$$

$$2\mathcal{P}_{\mathrm{L}}^{\mathrm{driv}} = \int \frac{dE}{h} D(E)\hbar\Omega k|c_{-k}|^2 (f_{\mathrm{R}}(E_k) - f_{\mathrm{L}}(E)). \tag{31}$$

The first contribution, $\mathcal{P}_{\mathrm{L}}^{\mathrm{pot}}$, is the dissipated power due to the dc current flowing in the presence of a potential bias. In the limit of no driving or in the limit of constant transmission $D(E) \equiv D_0$, where the ac driving averages out, this contribution equals the power dissipated in a steady-state system [35]. The second contribution, $\mathcal{P}_{\mathrm{L}}^{\mathrm{driv}}$, is the power that is dissipated due to the dc drive.

Also, the intersection bounds of Sec. III C and Appendix D take a simple form for the two-terminal system of Fig. 3. In particular, one finds for the integral contribution of the intersection bound (24),

$$\begin{aligned}&\int_{\varepsilon_{2n}}^{\varepsilon_{2n+2}} \frac{dE}{h}(f_\alpha^{\bigstar}(E) - f_\alpha(E)) \\ &\qquad \to \int_{\varepsilon_{2n}}^{\varepsilon_{2n+2}} \frac{dE}{h} D(E)(\tilde{f}_{\mathrm{R}}(E) - f_{\mathrm{L}}(E)),\end{aligned} \tag{32}$$

since $f_{\mathrm{L}}^{\bigstar}(E)$ and $\tilde{f}_{\mathrm{R}}(E)$ have the same crossing points with $f_{\mathrm{L}}(E)$ in the relevant energy intervals whenever $D(E) \neq 0$. The definition of $\tilde{f}_{\mathrm{R}}(E)$ is given in Eq. (27).

In the following, we discuss examples of specific drivings and transmission properties of the conductor.

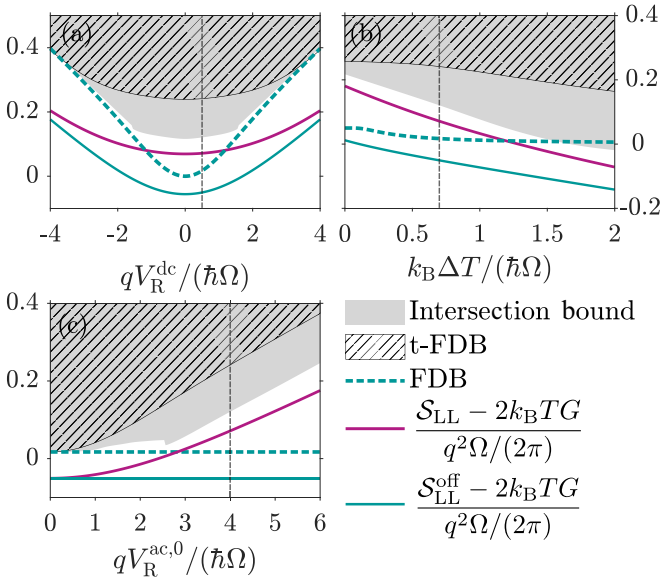

FIG. 4. Excess noise, $\mathcal{S}_{LL} - 2k_BTG$, see Eqs. (26) and (28), for a time-dependently driven system with constant transmission D_0 compared to the analogous system where the driving is switched off. Bounds on the excess noise are marked by filled regions for the driven case and as a dotted line when the driving is switched off. We show all results (a) as a function of the stationary bias voltage V_R^{dc} at $k_B\Delta T = 0.7\hbar\Omega$ and $qV_R^{ac,0} = 4\hbar\Omega$ [indicated by dashed vertical lines in (b) and (c)], (b) as a function of ΔT for $V_R^{dc} = 0.5\hbar\Omega$ and $qV_R^{ac,0} = 4\hbar\Omega$ [indicated by dashed vertical lines in (a) and (c)], and (c) as a function of $V_R^{ac,0}$ at $V_R^{dc} = 0.5\hbar\Omega$ and $k_B\Delta T = 0.7\hbar\Omega$ [indicated by dashed vertical lines in (a) and (b)]. In all panels, we furthermore fix $k_BT = 0.3\hbar\Omega$ and $D_0 = 0.1$.

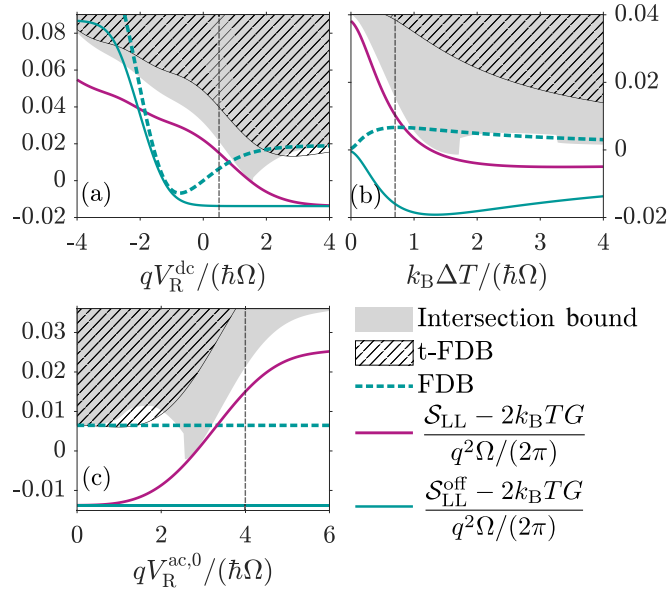

FIG. 5. Excess noise, $\mathcal{S}_{LL} - 2k_BTG$, see Eqs. (26) and (28), for a time-dependently driven system with boxcar-shaped transmission $D_{box}(E)$, with $D_0 = 0.1$, $E_0 = -2\hbar\Omega$ and $w = 1.5\hbar\Omega$, see Eq. (34), compared to the analogous system where the driving is switched off. All other parameters are chosen as in Fig. 4.

A. Harmonic driving

The results for the noise of the most simple case, namely, for a constant transmission $D(E) = D_0$ of the central conductor and in the presence of a cosine-shaped harmonic driving,

$$V_R^{ac,har} = V_R^{ac,0}\cos(\Omega t), \tag{33a}$$

are shown in Fig. 4. The Floquet coefficients incorporating the effect of this ac component of the potential are given by Bessel functions:

$$c_{-k}^{har} = J_{-k}\left(\frac{qV_R^{ac,0}}{\hbar\Omega}\right). \tag{33b}$$

We plot the noise as a function of the stationary biases for a fixed driving frequency and fixed driving amplitude in Figs. 4(a) and 4(b) and for fixed stationary biases as a function of the driving amplitude in Fig. 4(c). Black-striped regions indicate the noise values that are forbidden by the t-FDB, namely, the time-dependent fluctuation-dissipation bound (16), and gray-shaded regions those forbidden by the intersection bound (24). We observe that the intersection bound is here always tighter,[1] in particular, for small stationary biases and large driving amplitudes. This is to be expected since at low bias the hot reference distribution and the full effective, driven distribution intersect several times and—by construction—the intersection bound selects intervals in which the two distributions can be directly compared to each other. The intersection bound furthermore shows sharp steps, which are particularly visible as functions of the driving amplitude, Fig. 4(c), and are directly connected to crossings between distribution functions (see a detailed discussion of this in Appendix E).

We also show the result in the absence of time-dependent driving, here indicated by a superscript "off" for comparison. As expected, the fluctuation-dissipation bound found in Ref. [35] for systems in the absence of ac-driving, here denoted by FDB, breaks down when the frequency and the amplitude of the ac driving are sufficiently large compared to the stationary biases. Instead, for large stationary biases, the ac driving becomes less relevant, and the noise as well as the bounds in the ac-driven and non-ac-driven cases approach each other.

Until here, we have focused on a situation where the central conductor uniformly transmits or reflects particles incident at any energy. We now investigate the predictiveness of the bounds when an energy-dependent transmission filters particles at energies where the time-dependent driving is particularly relevant. In Fig. 5, we show the fluctuations as well as their fluctuation-dissipation and intersection bounds for the case of harmonic driving using a boxcar-shaped transmission probability for the central conductor,

$$D_{box}(E) = D_0\left(\Theta\left[E - E_0 + \frac{w}{2}\right] - \Theta\left[E - E_0 - \frac{w}{2}\right]\right), \tag{34}$$

[1]In other words, for *constant* transmission and the driving specifically chosen in Fig. 4, all regions excluded by the t-FDB are also excluded by the intersection bound but not vice versa.

where E_0 is the center of the boxcar and w its width. Due to the choice of the energy-filter position, the behavior of the noise is no longer symmetric around zero voltage bias; see Fig. 5(a). The energy filtering also reveals parameter regimes where the bounds are (close to) saturated, which strongly differ for the case of time-dependent driving compared to the static case (indicated by "off"). This is illustrated in, for instance, Fig. 5(a): at a positive voltage bias of approximately $V_{\mathrm{R}}^{\mathrm{dc}} \approx 1.5\hbar\Omega$, in particular, the intersection bound for the driven case saturates, whereas at a negative bias voltage of $V_{\mathrm{R}}^{\mathrm{dc}} \approx -\hbar\Omega$ the FDB for the static case saturates. That energy filtering can saturate the bounds is consistent with previous findings [35] in the stationary case, where the bounds were shown to approach equality for weak transmission and when transport takes place in energy intervals where the hot reference distribution is close to a constant value. More details are provided in Appendix E.

Furthermore, similarly to Fig. 4, there are extended parameter regimes in which the excess noise of the driven system breaks the FDB for the static case. In particular, it can be achieved for negative biases [Fig. 5(a)], at low temperature bias [Fig. 5(b)], or also at large driving amplitude [Fig. 5(c)]. This clearly shows the need for a dedicated bound for the time-dependent driving. Additionally, Fig. 5(a) shows that at large negative voltage biases the static excess noise exceeds both bounds for the time-dependent case.

In contrast with Fig. 4, the choice of an energy-dependent transmission function in Fig. 5 demonstrates the absence of a hierarchy, not only between the two different bounds for the time-dependently driven case, but also between the bound for the static case and the bounds for the time-dependently driven case. Indeed, while we have seen that the intersection bound is typically tighter, in Figs. 5(a) and 5(c) the t-FDB is lower than the intersection bound for some parameter regimes, namely for large voltage bias and driving amplitude, respectively.

B. Comparison of different ac-driving shapes

As a next step, we investigate how different driving shapes impact the noise and the bounds. We choose three specific driving potentials $V_{\mathrm{R}}^{\mathrm{ac}}(t)$ as examples to demonstrate the implications of the discovered bounds. They are (i) the most simple harmonic drive, with cosine shape $qV_{\mathrm{R}}^{\mathrm{ac,har}}(t)$ as discussed in the previous Sec. IV A, (ii) a Lorentzian drive, $qV_{\mathrm{R}}^{\mathrm{ac,Lor}}(t)$, which in the zero-temperature limit is known to have minimal excess noise [57–59], and (iii) a square drive, $qV_{\mathrm{R}}^{\mathrm{ac,squ}}(t)$, which instead has been shown to result in large excess noise [60]. These three signals are shown in Fig. 6(a). For case (i), where the ac driving potential in the right contact is given by a harmonic, see Eq. (33a), the Floquet coefficients are given in Eq. (33b). For a Lorentzian-shaped drive with one Lorentzian-shaped voltage peak per period, case (ii), where the pure ac component of the drive reads

$$V_{\mathrm{R}}^{\mathrm{ac,Lor}}(t) = V_{\mathrm{R}}^{\mathrm{ac},0} \sum_j \frac{\mathcal{T}\sigma/\pi}{(t - t_{\mathrm{Lor}} - j\mathcal{T})^2 + \sigma^2} - V_{\mathrm{R}}^{\mathrm{ac},0}, \quad (35a)$$

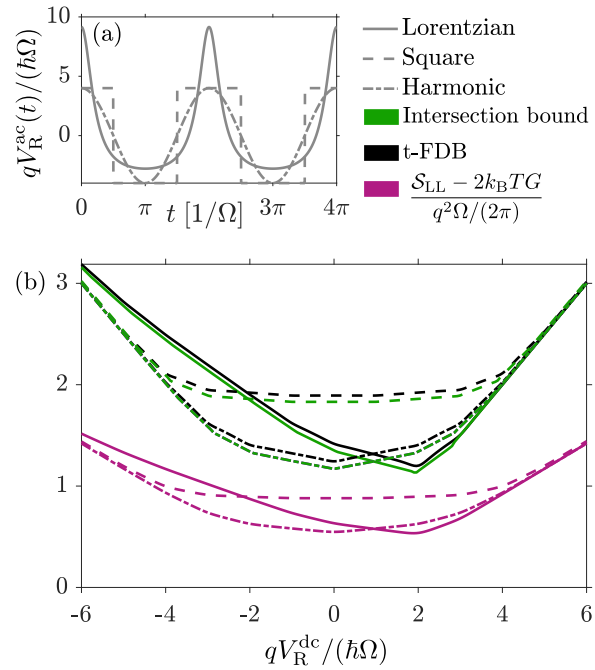

FIG. 6. Comparison of the effects of different driving schemes, as indicated in (a). (b) Excess noise and noise bounds as function of the stationary bias for these different driving shapes. We choose the parameters $k_{\mathrm{B}}T = 0.01\hbar\Omega$, $k_{\mathrm{B}}\Delta T = 0.1\hbar\Omega$, $D \equiv D_0 = 0.5$, and $qV_{\mathrm{R}}^{\mathrm{ac},0} = 4\hbar\Omega$. We furthermore have $\sigma = 0.1\mathcal{T}$ for the width of the Lorentzian pulses.

we instead have for its representation in terms of Floquet coefficients [47,59,60]:

$$c_{-k}^{\mathrm{Lor}} = \int_0^1 du \left(\frac{\sin[\pi(u + i\sigma/\mathcal{T})]}{\sin[\pi(u - i\sigma/\mathcal{T})]}\right)^{qV_{\mathrm{R}}^{\mathrm{ac},0}/\hbar\Omega} \times \exp\left[2\pi i u\left(-k - \frac{qV_{\mathrm{R}}^{\mathrm{ac},0}}{\hbar\Omega}\right)\right]. \quad (35b)$$

Finally, for case (iii), the Floquet coefficients for the ac component of a square drive with

$$V_{\mathrm{R}}^{\mathrm{ac,squ}}(t) = V_{\mathrm{R}}^{\mathrm{ac},0}\mathrm{sgn}[\cos(\Omega t)] \quad (36a)$$

are given by [60]

$$c_{-k}^{\mathrm{squ}} = \frac{2}{\pi}\frac{qV_{\mathrm{R}}^{\mathrm{ac},0}/\Omega}{k^2 - \left(qV_{\mathrm{R}}^{\mathrm{ac},0}/\Omega\right)^2}\sin\left[\frac{\pi}{2}\left(-k - qV_{\mathrm{R}}^{\mathrm{ac},0}/\Omega\right)\right]. \quad (36b)$$

We choose a low-temperature regime to highlight the characteristic features of the different drivings. Indeed, as expected, there are regions where the Lorentzian driving outperforms the harmonic driving by displaying the lowest noise level in excess to the thermal noise—here occurring at $V_{\mathrm{R}}^{\mathrm{dc}} \approx 2\hbar\Omega$. Also as expected, the square drive is the driving scheme that generates the highest level of excess noise [60]. These properties of the noise are also reflected in the shape of the fluctuation-dissipation bound and the intersection bound. However, the bounds are far from being tight in the parameter regime chosen here to highlight the differences in the excess noise between different driving scheme. This large difference

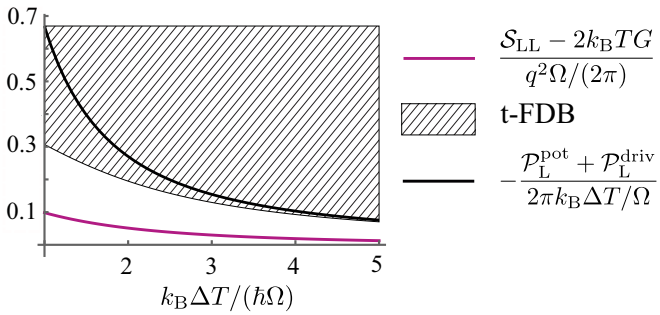

FIG. 7. Excess noise, t-FDB [see Eq. (16)], and t-FDB in the limit of large temperature bias, $\Delta T \gg \Delta\mu + \hbar\Omega k$ expressed in terms of dissipated power [Eq. (22)]. The driving has cosine shape with $qV_R^{ac,0} = 2\hbar\Omega$. The boxcar-shaped transmission probability has $D_0 = 1$, $E_0 = 3\hbar\Omega$ and $w = \hbar\Omega$. We furthermore have $qV_R^{dc} = 3\hbar\Omega$ and $k_BT = \hbar\Omega$.

between excess noises and their bounds can be ascribed to the fact that we here choose an energy-independent transmission of significant magnitude (where we expect the t-FDB to be least tight, as confirmed by the analysis of the static case [35]) in order not to mix features of driving and of energy filtering and to evidence the difference in the driving schemes.

The characteristics associated to the different driving schemes disappear rather rapidly with increasing voltage bias or with increasing temperature bias (not shown here). For large biases, the noises and bounds would also approach the results for the nondriven case; see Fig. 4(a) for comparison. This demonstrates that—in the simple two-terminal setup with ac-voltage bias driving—the shape of the driving signal has a less important impact on the noise bounds than for example the energy filtering of the central conductor discussed above in Sec. IV A.

C. Relation of noise bounds to power production

Finally, we demonstrate the relation between the t-FDB and the dissipated powers due to static bias voltage and driving, see (22), for the example of the two-terminal conductor driven by a harmonic ac potential in the terminals, as shown in Fig. 3, and discussed in Sec. IV A. The explicit expressions are given in Eq. (26) for the noise and in Eqs. (30) and (31) for the power.

The excess noise of the driven system is shown in Fig. 7 together with the full t-FDB (16) and its limit for large temperature differences which directly relates to the dissipated powers (22). We see that the large ΔT approximation, namely, the sum of dissipated powers divided by the temperature difference, approaches the t-FDB already at temperature differences of the order of $\Delta T \approx 3.5\hbar\Omega$. While the excess noise is suppressed, tending to zero, in this limit, the full t-FDB, Eq. (18), as well as the large-temperature limit of the t-FDB expressed in terms of dissipated powers, Eq. (22), still describe the overall behavior and yield reasonable estimations of the excess noise. This shows that the t-FDB bound for large temperature biases (22), which does not require any information about the Floquet decomposition of the current but bounds the noise by the power, constitutes a good estimate for the noise in large parameter regimes.

V. CONCLUSIONS

We have derived bounds on the excess noise of generic time-dependently driven electronic coherent conductors, which are furthermore subject to possibly large static voltage and temperature biases. The first of these bounds, referred to as the fluctuation-dissipation bound for time-dependently driven systems (16), admits an intuitive interpretation in terms of power dissipated by the time-dependent driving and the static biases (22), which is particularly predictive in the regime of large temperature bias. A second bound, referred to as intersection bound (24), relies on knowledge about the crossing points between (effective) distribution functions. We expect that this intersection bound is of use for the characterization of noise in systems with generic nonthermal distributions, i.e., not necessarily stemming from time-dependent driving [61]. In the absence of driving (or other nonthermal effects), both bounds tend to the static fluctuation-dissipation bound, previously developed in Ref. [35].

We have demonstrated the validity of the bounds and highlighted their characteristic features for the simple but experimentally relevant [59,62,63] example case of a two-terminal out-of equilibrium conductor subject to an ac bias voltage. However, the validity of the presented bounds extends far beyond this case. We expect the bounds to be useful to understand and to constrain, e.g., the noise of periodically operated heat engines [64] and of single-electron sources in the presence of (accidental) temperature gradients.

In the future, it would be interesting to explore extensions of the developed bounds for transient (nonperiodic) dynamics, finite-frequency noise, and systems with strong Coulomb interactions, which cannot be covered by the Floquet scattering approach chosen here.

ACKNOWLEDGMENTS

We thank R. Sánchez and E. Danielsson for helpful discussions throughout the duration of the project and M. Acciai for providing useful feedback on the manuscript. We gratefully acknowledge funding from the Knut and Alice Wallenberg Foundation via the Fellowship program and from the European Research Council (ERC) under the European Union's Horizon Europe research and innovation program (101088169/NanoRecycle) (L.T. and J.S.) as well as from the Spanish Ministerio de Ciencia e Innovación via Grants No. PID2019-110125GB-I00, No. PID2022-142911NB-I00, and No. PID2024-157821NB-I00 (J.B.).

DATA AVAILABILITY

The data that support the findings of this article are not publicly available. The data are available from the authors upon reasonable request.

APPENDIX A: PROPERTIES OF FLOQUET SCATTERING MATRIX

In this appendix, we show some of the important properties of the scattering matrix and the Floquet coefficients.

1. Floquet coefficients

The Floquet coefficients fulfill some important properties. To show them, we start from the definitions in Eqs. (4). First, we demonstrate the sum rule

$$\begin{aligned}\sum_k c^*_{\alpha(k+p)}c_{\alpha(k+\ell)} &= \int_0^{\mathcal{T}}\frac{dt}{\mathcal{T}}\int_0^{\mathcal{T}}\frac{dt'}{\mathcal{T}}\sum_k e^{i\phi_\alpha(t')}e^{-i(k+p)\Omega t'}e^{-i\phi_\alpha(t)}e^{i(k+\ell)\Omega t}\\ &= \int_0^{\mathcal{T}}\frac{dt}{\mathcal{T}}e^{-i(p-\ell)\Omega t} = \delta_{p\ell}. \end{aligned} \tag{A1}$$

Furthermore, we demonstrate a relation needed to express the components of the driving potential in terms of Floquet coefficients

$$\sum_k kc^*_{\alpha(k-p)}c_{\alpha k} = \int_0^{\mathcal{T}}\frac{dt'}{\mathcal{T}}\int_0^{\mathcal{T}}\frac{dt}{\mathcal{T}}e^{i\phi_\alpha(t')-i\phi_\alpha(t)}\sum_k ke^{ik\Omega t}e^{-i(k-p)\Omega t'}.$$

Rewriting the factor k as a derivative of the exponential $e^{ik\Omega t}$ and integrating by parts while using the periodicity of the driving potential, we find

$$\begin{aligned}\sum_k kc^*_{\alpha(k-p)}c_{\alpha k} &= \int_0^{\mathcal{T}}\frac{dt'}{\mathcal{T}}\int_0^{\mathcal{T}}\frac{dt}{\mathcal{T}}e^{i\phi_\alpha(t')-i\phi_\alpha(t)}\\ &\quad\times\sum_k\frac{q}{\hbar\Omega}V^{\mathrm{ac}}_\alpha(t)e^{ik\Omega t}e^{-i(k-p)\Omega t'}\\ &= \frac{q}{\hbar\Omega}\int_0^{\mathcal{T}}\frac{dt}{\mathcal{T}}\sum_n V_{\alpha n}e^{-in\Omega t}e^{ip\Omega t}\\ &= \frac{q}{\hbar\Omega}V_{\alpha p}. \end{aligned} \tag{A2}$$

This result directly implies

$$\sum_k k|c_{\alpha,k}|^2 = 0. \tag{A3}$$

2. Unitarity of Floquet scattering matrix

The Floquet scattering matrix fulfills the unitarity condition

$$\sum_{\beta,p}\tilde{t}^\dagger_{\alpha\beta}(E_\ell,E_p)\tilde{t}_{\alpha\beta}(E_k,E_p) = \delta_{k\ell}\mathbf{1}_\alpha, \tag{A4}$$

here written for the submatrices $\tilde{t}_{\alpha\beta}$ with $[\tilde{t}_{\alpha\beta}]_{nm} = \tilde{s}_{\alpha n,\beta m}$, with $\mathbf{1}_\alpha$ the unit matrix of dimension N_α.

APPENDIX B: POWER DUE TO DRIVING AND STATIC BIASES

We need the expressions for the power to interpret the t-FDB, namely, the fluctuation-dissipation bound with time-dependent driving. We start by writing the energy current in the driven system flowing into contact α, which is given by

$$\begin{aligned}I^E_\alpha &= \int dE\,\frac{E}{h}\sum_{\beta,k}\mathrm{Tr}\{\tilde{t}^\dagger_{\alpha\beta}(E,E_k)\tilde{t}_{\alpha\beta}(E,E_k)\}\\ &\quad\times(f_\beta(E_k)-f_\alpha(E)). \end{aligned} \tag{B1}$$

The sum over all energy currents yields the total power provided by the driving and dissipated in the system. This is equivalent to minus the power received by the driving. To find this received power, $\mathcal{P}^{\mathrm{driv}}$, we first rewrite the negative of the sum over energy currents using the unitarity of the scattering matrix

$$\begin{aligned}\mathcal{P}^{\mathrm{driv}} &= -\sum_\alpha I^E_\alpha = -\sum_\alpha\int dE\,\frac{E}{h}\\ &\quad\times\left[\sum_{\beta,k}\mathrm{Tr}\{\tilde{t}^\dagger_{\alpha\beta}(E,E_k)\tilde{t}_{\alpha\beta}(E,E_k)\}f_\beta(E_k) - N_\alpha f_\alpha(E)\right]\\ &= \sum_{\alpha,\beta,k}\int dE\,\frac{E}{h}(\mathrm{Tr}\{\tilde{t}^\dagger_{\beta\alpha}(E_k,E)\tilde{t}_{\beta\alpha}(E_k,E)\}f_\alpha(E)\\ &\quad-\mathrm{Tr}\{\tilde{t}^\dagger_{\alpha\beta}(E,E_k)\tilde{t}_{\alpha\beta}(E,E_k)\}f_\beta(E_k)). \end{aligned} \tag{B2}$$

As a next step, we shift the energy $E\to E_{-k}$ and swap the indices $k\to -k$ and $\alpha\leftrightarrow\beta$, which results in

$$\begin{aligned}&\sum_{\alpha,\beta,k}\int dE\,\frac{E_k}{h}(\mathrm{Tr}\{\tilde{t}^\dagger_{\alpha\beta}(E,E_k)\tilde{t}_{\alpha\beta}(E,E_k)\}f_\beta(E_k)\\ &\quad-\mathrm{Tr}\{\tilde{t}^\dagger_{\beta\alpha}(E_k,E)\tilde{t}_{\beta\alpha}(E_k,E)\}f_\alpha(E)). \end{aligned} \tag{B3}$$

Summing now the identical expressions (B2) and (B3) and dividing by 2, we find the power $\mathcal{P}^{\mathrm{driv}}$ as

$$\begin{aligned}\mathcal{P}^{\mathrm{driv}} &= \sum_{\alpha,\beta,k}\int dE\,\frac{k\Omega}{4\pi}(\mathrm{Tr}\{\tilde{t}^\dagger_{\alpha\beta}(E,E_k)\tilde{t}_{\alpha\beta}(E,E_k)\}f_\beta(E_k)\\ &\quad-\mathrm{Tr}\{\tilde{t}^\dagger_{\beta\alpha}(E_k,E)\tilde{t}_{\beta\alpha}(E_k,E)\}f_\alpha(E)). \end{aligned} \tag{B4}$$

In the same way, one can derive the power received by the time-reversed protocol, exploiting the behavior of the Floquet scattering matrix under time reversal, $[\tilde{t}_{\alpha\beta}(E,E_k)]^{\mathrm{tr}} = \tilde{t}_{\beta\alpha}(E_k,E)$; see Ref. [65] and p. 73 in Ref. [47]. One then finds

$$\begin{aligned}\mathcal{P}^{\mathrm{driv,tr}} &:= \sum_{\alpha,\beta,k}\int dE\,\frac{k\Omega}{4\pi}(\mathrm{Tr}\{\tilde{t}^\dagger_{\beta\alpha}(E_k,E)\tilde{t}_{\beta\alpha}(E_k,E)\}f_\beta(E_k)\\ &\quad-\mathrm{Tr}\{\tilde{t}^\dagger_{\alpha\beta}(E,E_k)\tilde{t}_{\alpha\beta}(E,E_k)\}f_\alpha(E)). \end{aligned} \tag{B5}$$

We can proceed in a similar way to find the power generated in contact α due to a current flowing in the presence of static voltage biases. Thus, we start from a sum over all heat currents in contact α, which are given by $J_\alpha = I^E_\alpha - \mu_\alpha I^N_\alpha$. We have already shown how the sum over all energy currents yields the power dissipated due to the driving or received by the driving fields. The power *produced* by the part of the energy current stemming from the chemical work is given by

$$\begin{aligned}\mathcal{P}^{\mathrm{pot}} &= \sum_\alpha\mu_\alpha I^N_\alpha = -\sum_{\alpha,\beta,k}\frac{\mu_\alpha}{h}\int dE\\ &\quad\times\mathrm{Tr}\{\tilde{t}^\dagger_{\alpha\beta}(E,E_k)\tilde{t}_{\alpha\beta}(E,E_k)\}(f_\beta(E_k)-f_\alpha(E)). \end{aligned} \tag{B6}$$

For the power generated in the time-reversed situation, we instead find

$$\begin{aligned}\mathcal{P}^{\mathrm{pot,tr}} &= \sum_{\alpha,\beta,k}\frac{\mu_\alpha}{h}\int dE\ \mathrm{Tr}\{\tilde{t}^\dagger_{\beta\alpha}(E_k,E)\tilde{t}_{\beta\alpha}(E_k,E)\}\\ &\quad\times(f_\beta(E_k)-f_\alpha(E))\\ &= \sum_{\alpha,\beta,k}\frac{\mu_\beta}{h}\int dE\ \mathrm{Tr}\{\tilde{t}^\dagger_{\alpha\beta}(E,E_k)\tilde{t}_{\alpha\beta}(E,E_k)\}\\ &\quad\times(f_\alpha(E)-f_\beta(E_k)),\end{aligned}\tag{B7}$$

where we swapped indices and shifted energies in the second line of Eq. (B7).

APPENDIX C: DERIVATION OF THE T-FDB

To derive the t-FDB, namely, the fluctuation-dissipation bound in the presence of time-dependent driving, we have split the noise in the three contributions $\mathcal{S}^{(0)}_{\alpha\alpha}$, $\mathcal{S}^{(2)}_{\alpha\alpha}$, and $\mathcal{S}^{(4)}_{\alpha\alpha}$ in Eq. (12). We have written $\mathcal{S}^{(2)}_{\alpha\alpha}$ in terms of the linear conductance and a contribution that partially cancels out with $\mathcal{S}^{(0)}_{\alpha\alpha}$ in Eq. (13). Here, we show how to rewrite and estimate the remaining contributions from $\mathcal{S}^{(0)}_{\alpha\alpha}$ and, in particular, from $\mathcal{S}^{(4)}_{\alpha\alpha}$. First, we split the contribution $\mathcal{S}^{(4)}_{\alpha\alpha}$ into two pieces, one linear in the Fermi functions $\mathcal{S}^{(4,1)}_{\alpha\alpha}$ and one quadratic in the Fermi functions $\mathcal{S}^{(4,2)}_{\alpha\alpha}$. The scalar product nature of the latter,

$$\begin{aligned}\mathcal{S}^{(4,2)}_{\alpha\alpha} &= -\frac{q^2}{h}\int dE f_\beta(E_k)f_\gamma(E_p)\\ &\quad\times\mathrm{Tr}\{\tilde{t}_{\alpha\beta}(E_\ell,E_k)\tilde{t}^\dagger_{\alpha\beta}(E,E_k)\tilde{t}_{\alpha\gamma}(E,E_p)\tilde{t}^\dagger_{\alpha\gamma}(E_\ell,E_p)\},\end{aligned}\tag{C1}$$

allows us to use the Cauchy-Schwarz inequality, such that

$$\mathcal{S}^{(4,2)}_{\alpha\alpha}\leqslant-\frac{q^2}{hN_\alpha}\int dE|\mathrm{Tr}\{\tilde{t}_{\alpha\beta}(E,E_k)\tilde{t}^\dagger_{\alpha\beta}(E,E_k)\}f_\beta(E_k)|^2.\tag{C2}$$

To be able to further treat this term, we add and subtract $f_\alpha(E)$ from $f_\beta(E_k)$ to find

$$\begin{aligned}\mathcal{S}^{(4,2)}_{\alpha\alpha} &\leqslant -\frac{q^2}{h}\int dE N_\alpha f_\alpha(E)f_\alpha(E)\\ &\quad-\frac{q^2}{hN_\alpha}\int dE|\mathrm{Tr}\{\tilde{t}_{\alpha\beta}(E,E_k)\tilde{t}^\dagger_{\alpha\beta}(E,E_k)\}\\ &\quad\times(f_\beta(E_k)-f_\alpha(E))|^2\\ &\quad-2\frac{q^2}{h}\int dE\mathrm{Tr}\{\tilde{t}_{\alpha\beta}(E,E_k)\tilde{t}^\dagger_{\alpha\beta}(E,E_k)\}\\ &\quad\times f_\alpha(E)(f_\beta(E_k)-f_\alpha(E)).\end{aligned}\tag{C3}$$

We note here that the first term will cancel with parts of $\mathcal{S}^{(0)}$, respectively, $\mathcal{S}^{(2)}$, while the second one is finite but always negative. As a next step, before summing together all contributions, we now analyze $\mathcal{S}^{(4,1)}$, which reads

$$\begin{aligned}\mathcal{S}^{(4,1)}_{\alpha\alpha} &= \frac{q^2}{h}\int dE f_\beta(E_k)\\ &\quad\times\mathrm{Tr}\{\tilde{t}_{\alpha\beta}(E_\ell,E_k)\tilde{t}^\dagger_{\alpha\beta}(E,E_k)\tilde{t}_{\alpha\gamma}(E,E_p)\tilde{t}^\dagger_{\alpha\gamma}(E_\ell,E_p)\}\\ &= \frac{q^2}{h}\int dE f_\beta(E_k)\mathrm{Tr}\{\tilde{t}_{\alpha\beta}(E,E_k)\tilde{t}^\dagger_{\alpha\beta}(E,E_k)\}.\end{aligned}\tag{C4}$$

Here we again subtract and add $f_\alpha(E)$ to find

$$\begin{aligned}\mathcal{S}^{(4,1)}_{\alpha\alpha} &= \frac{q^2}{h}\int dE N_\alpha f_\alpha(E)\\ &\quad+\frac{q^2}{h}\int dE(f_\beta(E_k)-f_\alpha(E))\\ &\quad\times\mathrm{Tr}\{\tilde{t}_{\alpha\beta}(E,E_k)\tilde{t}^\dagger_{\alpha\beta}(E,E_k)\}.\end{aligned}\tag{C5}$$

Now summing $\mathcal{S}^{(0)}_{\alpha\alpha}$, $\mathcal{S}^{(2)}_{\alpha\alpha}$, and $\mathcal{S}^{(4,1)}_{\alpha\alpha}$ to the inequality developed starting from $\mathcal{S}^{(4,2)}_{\alpha\alpha}$ in (C3), we reach the bound presented in (14) in the main text.

APPENDIX D: ALTERNATIVE INTERSECTION BOUND

In Sec. III C, we have presented a noise bound that is based on intersections between effective distribution functions. The shape of this bound hence heavily depends on how the effective distribution functions are defined. An alternative way to write a bound, in which the currentlike shape of the bound contributions is highlighted, is by introducing the effective distribution function

$$f^\star_\alpha(E)=\frac{\sum_{(\beta,k)\notin\{(\alpha,0)\}}\mathrm{Tr}\{\tilde{t}_{\alpha\beta}(E,E_k)\tilde{t}^\dagger_{\alpha\beta}(E,E_k)\}f_\beta(E_k)}{\sum_{(\beta,k)\notin\{(\alpha,0)\}}\mathrm{Tr}\{\tilde{t}_{\alpha\beta}(E,E_k)\tilde{t}^\dagger_{\alpha\beta}(E,E_k)\}},\tag{D1}$$

which is well-defined as long as $\mathrm{Tr}\{\tilde{t}_{\alpha\beta}(E,E_k)\tilde{t}^\dagger_{\alpha\beta}(E,E_k)\}\neq 0$ for at least one $(\beta,k)\notin\{(\alpha,0)\}$. This modified distribution function $f^\star_\alpha(E)$, when defined on the entire energy interval, has M crossings with the hottest distribution $f_\alpha(E)$, which are the same crossings as the one between $f^\bigstar_\alpha(E)$ and $f_\alpha(E)$. With this, we can write the intersection bound as

$$\begin{aligned}\mathcal{S}_{\alpha\alpha}-2k_\mathrm{B}T_\alpha\sum_{\beta\neq\alpha}G_{\alpha\beta} &\leqslant q^2\sum_{n=0}^{\frac{M-1}{2}}(1-2f_\alpha(\varepsilon_{2n+1}))\\ &\quad\times\int_{\varepsilon_{2n}}^{\varepsilon_{2n+2}}\frac{dE}{h}D_\alpha(E)(f^\star_\alpha(E)-f_\alpha(E)).\end{aligned}\tag{D2}$$

Here, the factor $D_\alpha(E)=N_\alpha-\mathrm{Tr}\{t^\dagger_{\alpha\alpha}(E)t_{\alpha\alpha}(E)\}$ can be understood as a transmission probability for a current resulting from the difference in occupations $f^\star_\alpha(E)-f_\alpha(E)$ in the interval $[\varepsilon_{2n},\varepsilon_{2n+2}]$.

For the example treated in Sec. IV, $f^\star_\mathrm{L}(E)$ equals $\tilde{f}_\mathrm{R}(E)$ on the support of $D(E)$, but $\tilde{f}_\mathrm{R}(E)$ is also defined when $D(E)=0$.

APPENDIX E: INTERSECTIONS BETWEEN DISTRIBUTION FUNCTIONS

In this appendix, we demonstrate how a number of features in the bounds, observed in Figs. 4 and 5, can be explained

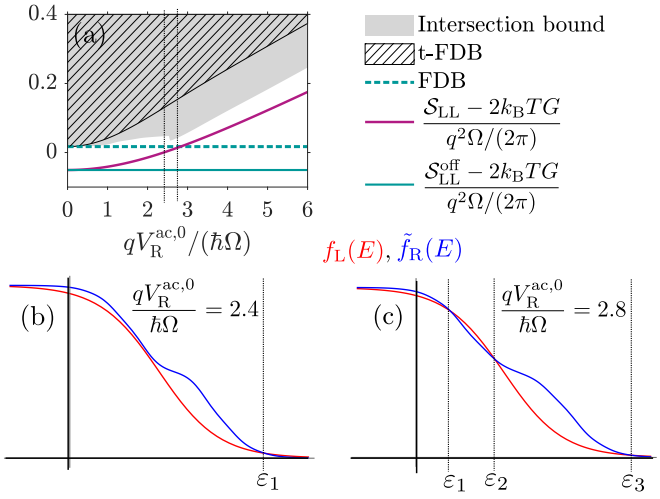

FIG. 8. Excess noise and bounds for a harmonically driven two-terminal conductor with constant transmission probability [all parameters in (a) as in Fig. 4(c) in the main text]. (b), (c) Distribution function for the hot contact (red) and the modified distribution from the cold contact due to driving (blue) at the parameter values indicated by vertical dashed lines in (a), namely, at $qV_{\rm R}^{\rm ac,0} = 2.4\hbar\Omega$ in (b) and at $qV_{\rm R}^{\rm ac,0} = 2.8\hbar\Omega$ in (c).

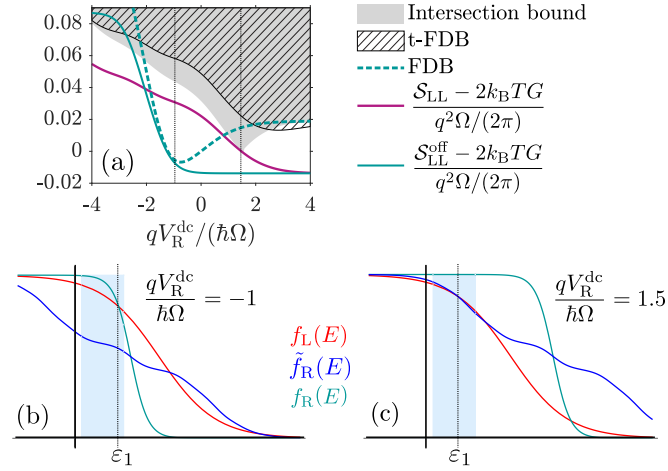

FIG. 9. Excess noise and bounds for a harmonically driven two-terminal conductor with box-car shaped transmission probability $D_{\rm box}(E)$ [all parameters in (a) as in Fig. 5(a) in the main text]. (b), (c) Distribution function for the hot contact (red) of the modified distribution from the cold contact due to driving (blue), and the cold contact in the absence of driving (cyan) at the parameter values indicated by vertical dashed lines in (a), namely, at $qV_{\rm R}^{\rm dc} = -\hbar\Omega$ in (b) and at $qV_{\rm R}^{\rm dc} = 1.5\hbar\Omega$ in (c).

by examining the relevant crossings between effective driven distributions and the reference distribution of the hot reservoir. For simplicity, we here always show $\tilde{f}_{\rm R}(E)$, see Eq. (27), instead of $f_{\rm L}^{\star}(E)$, see Eq. (23). This simplifies the plots and the discussion, while the crossing points remain the same.

1. Sharp features in intersection bound

In Figs. 4 and 5, the intersection bound displays discontinuities as function of different externally tunable parameters. This can be explained by examining how crossings between the hot reference distribution and the effective distribution of the driven contact appear and disappear as function of those parameters.

In Fig. 8, we show this for the intersection bound as function of the driving amplitude in the case of harmonic driving and energy-independent transmission; see also Fig. 4(c). We show the effective distribution functions $\tilde{f}_{\rm R}(E)$ for two values of the driving amplitude in the vicinity of the sharp step in the intersection bound. Indeed, two additional crossing points, indicated by ε_1, ε_2 occur, when changing $V_{\rm R}^{\rm ac,0}$ from $2.4\hbar\Omega$ to $2.8\hbar\Omega$.

2. Crossing points and energy-dependent transmission

How tight the different bounds are and in which hierarchy they occur depends strongly on the energy-filtering properties of the transmission functions, as can be observed when comparing Fig. 4 with 5. We show this for two different parameter sets and the related distribution function in Fig. 9.

At $qV_{\rm R}^{\rm dc} = -\hbar\Omega$, indicated by the left vertical dashed line in Fig. 9(a), the excess noise of the time-dependently driven system breaks the static FDB while the t-FDB and intersection bounds remain valid. Also, the static bound has an opposite sign compared to the bounds in the presence of driving. Figure 9(b) shows the relevant distribution function, where the region selected by the box-car-shaped energy filter is highlighted in light blue. Indeed, when comparing the reference hot distribution with the distribution of the right, colder contact, one notices that for the driven case the effective cold distribution $\tilde{f}_{\rm R}(E)$ is smaller than the hot reference distribution, while for the static case, the cold distribution $f_{\rm R}(E)$ is larger than the hot one. This means that their relative magnitudes are inverted within the energy window selected by the filter, when comparing the driven and static case. Also, the cold distribution of the static system (cyan) is much closer to the hot distribution than the modified cold distribution of the driven system (blue). Therefore the static and the time-dependently driven case are expected to behave fundamentally different. The static FDB is close to zero, while the t-FDB and intersection bounds are positive and larger, such that the excess noise in the driven case can break the static bound.

Instead, at $qV_{\rm R}^{\rm dc} = 1.5\hbar\Omega$, indicated by the right vertical dashed line in Fig. 9(a), the intersection bound is close to zero. Indeed, analyzing the distribution functions at this point shows that the energy filter exactly selects the interval around the crossing points between the effective driven distribution and the hot reference distribution, where the two distributions are furthermore very similar.

In both cases, the energy filter $D(E)$ selects a rather small window of the hot distribution, $w \ll k_{\rm B}T_{\rm L}$, such that the (hot reference) distribution assumes a close to constant value $f_{\rm L}(E) \approx f_{\rm L}(\varepsilon_1)$ in the relevant energy interval. The bounds in both indicated situations are therefore relatively tight; see also the derivation of the bounds in Sec. III A.

[1] G. Benenti, G. Casati, K. Saito, and R. S. Whitney, Fundamental aspects of steady-state conversion of heat to work at the nanoscale, Phys. Rep. **694**, 1 (2017).

[2] R. S. Whitney, R. Sánchez, and J. Splettstoesser, Quantum thermodynamics of nanoscale thermoelectrics and electronic devices, *Thermodynamics in the Quantum Regime* (Springer, Cham, Switzerland, 2019), pp. 175–206.

[3] L. M. Cangemi, C. Bhadra, and A. Levy, Quantum engines and refrigerators, Phys. Rep. **1087**, 1 (2024).

[4] J. Balduque and R. Sánchez, Quantum thermocouples: Nonlocal conversion and control of heat in nanostructures, Eur. Phys. J. Spec. Top. 1 (2026).

[5] F. Giazotto, T. T. Heikkilä, A. Luukanen, A. M. Savin, and J. P. Pekola, Opportunities for mesoscopics in thermometry and refrigeration: Physics and applications, Rev. Mod. Phys. **78**, 217 (2006).

[6] J. P. Pekola, O.-P. Saira, V. F. Maisi, A. Kemppinen, M. Möttönen, Y. A. Pashkin, and D. V. Averin, Single-electron current sources: Toward a refined definition of the ampere, Rev. Mod. Phys. **85**, 1421 (2013).

[7] H. Edlbauer, J. Wang, T. Crozes, P. Perrier, S. Ouacel, C. Geffroy, G. Georgiou, E. Chatzikyriakou, A. Lacerda-Santos, X. Waintal, D. Christian Glattli, P. Roulleau, J. Nath, M. Kataoka, J. Splettstoesser, M. Acciai, M. C. da Silva Figueira, K. Öztas, A. Trellakis, T. Grange, *et al.*, Semiconductor-based electron flying qubits: Review on recent progress accelerated by numerical modelling, EPJ Quantum Technol. **9**, 21 (2022).

[8] M. Acciai, L. Arrachea, and J. Splettstoesser, Quantum transport phenomena induced by time-dependent fields, Riv. Nuovo Cim. **48**, 653 (2025).

[9] Ya. M. Blanter and M. Büttiker, Shot noise in mesoscopic conductors, Phys. Rep. **336**, 1 (2000).

[10] K. Kobayashi and M. Hashisaka, Shot noise in mesoscopic systems: From single particles to quantum liquids, J. Phys. Soc. Jpn. **90**, 102001 (2021).

[11] H. B. Callen and T. A. Welton, Irreversibility and generalized noise, Phys. Rev. **83**, 34 (1951).

[12] M. S. Green, Markoff random processes and the statistical mechanics of time-dependent phenomena. II. Irreversible processes in fluids, J. Chem. Phys. **22**, 398 (1954).

[13] R. Kubo, Statistical-mechanical theory of irreversible processes. I. General theory and simple applications to magnetic and conduction problems, J. Phys. Soc. Jpn. **12**, 570 (1957).

[14] M. Esposito, U. Harbola, and S. Mukamel, Nonequilibrium fluctuations, fluctuation theorems, and counting statistics in quantum systems, Rev. Mod. Phys. **81**, 1665 (2009).

[15] D. Rogovin and D. J. Scalapino, Fluctuation phenomena in tunnel junctions, Ann. Phys. **86**, 1 (1974).

[16] L. S. Levitov and M. Reznikov, Counting statistics of tunneling current, Phys. Rev. B **70**, 115305 (2004).

[17] D. Andrieux and P. Gaspard, Fluctuation theorem for transport in mesoscopic systems, J. Stat. Mech. (2006) P01011.

[18] I. Safi, Time-dependent transport in arbitrary extended driven tunnel junctions, arXiv:1401.5950 .

[19] R.-P. Riwar and J. Splettstoesser, Transport fluctuation relations in interacting quantum pumps, New J. Phys. **23**, 013010 (2021).

[20] B. Altaner, M. Polettini, and M. Esposito, Fluctuation-dissipation relations far from equilibrium, Phys. Rev. Lett. **117**, 180601 (2016).

[21] N. Shiraishi, Time-symmetric current and its fluctuation response relation around nonequilibrium stalling stationary state, Phys. Rev. Lett. **129**, 020602 (2022).

[22] J. Tobiska and Yu. V. Nazarov, Inelastic interaction corrections and universal relations for full counting statistics in a quantum contact, Phys. Rev. B **72**, 235328 (2005).

[23] H. Förster and M. Büttiker, Fluctuation relations without microreversibility in nonlinear transport, Phys. Rev. Lett. **101**, 136805 (2008).

[24] Y. Utsumi, D. S. Golubev, M. Marthaler, K. Saito, T. Fujisawa, and G. Schön, Bidirectional single-electron counting and the fluctuation theorem, Phys. Rev. B **81**, 125331 (2010).

[25] G. T. Landi, M. J. Kewming, M. T. Mitchison, and P. P. Potts, Current fluctuations in open quantum systems: Bridging the gap between quantum continuous measurements and full counting statistics, PRX Quantum **5**, 020201 (2024).

[26] A. C. Barato and U. Seifert, Thermodynamic uncertainty relation for biomolecular processes, Phys. Rev. Lett. **114**, 158101 (2015).

[27] T. R. Gingrich, J. M. Horowitz, N. Perunov, and J. L. England, Dissipation bounds all steady-state current fluctuations, Phys. Rev. Lett. **116**, 120601 (2016).

[28] I. Di Terlizzi and M. Baiesi, Kinetic uncertainty relation, J. Phys. A: Math. Theor. **52**, 02LT03 (2018).

[29] K. Brandner, T. Hanazato, and K. Saito, Thermodynamic bounds on precision in ballistic multiterminal transport, Phys. Rev. Lett. **120**, 090601 (2018).

[30] D. Palmqvist, L. Tesser, and J. Splettstoesser, Kinetic uncertainty relations for quantum transport, Phys. Rev. Lett. **135**, 166302 (2025).

[31] D. Palmqvist, L. Tesser, and J. Splettstoesser, Combining kinetic and thermodynamic uncertainty relations in quantum transport, Quantum Sci. Technol. **10**, 035059 (2025).

[32] K. Brandner and K. Saito, Thermodynamic uncertainty relations for coherent transport, Phys. Rev. Lett. **135**, 046302 (2025).

[33] A. M. Timpanaro, G. Guarnieri, and G. T. Landi, Quantum thermoelectric transmission functions with minimal current fluctuations, Phys. Rev. B **111**, 014301 (2025).

[34] K. Brandner and K. Saito, Thermodynamic bound on current fluctuations in coherent conductors, J. Phys. A: Math. Theor. **58**, 435002 (2025).

[35] L. Tesser and J. Splettstoesser, Out-of-equilibrium fluctuation-dissipation bounds, Phys. Rev. Lett. **132**, 186304 (2024).

[36] O. Pan, Z. Fan, S. Zhang, J. Li, J. Chen, and S. Su, Fluctuation-dissipation limits in quantum thermoelectric transport, arXiv:2601.06984.

[37] E. Potanina, C. Flindt, M. Moskalets, and K. Brandner, Thermodynamic bounds on coherent transport in periodically driven conductors, Phys. Rev. X **11**, 021013 (2021).

[38] J. Lu, Z. Wang, J. Peng, C. Wang, J.-H. Jiang, and J. Ren, Geometric thermodynamic uncertainty relation in a periodically driven thermoelectric heat engine, Phys. Rev. B **105**, 115428 (2022).

[39] L. Tesser, M. Acciai, C. Spånslätt, I. Safi, and J. Splettstoesser, Thermodynamic and energetic constraints on transition probabilities of small-scale quantum systems, Phys. Rev. Res. **7**, 023084 (2025).

[40] P. Portugal, F. Brange, and C. Flindt, Heat pulses in electron quantum optics, Phys. Rev. Lett. **132**, 256301 (2024).
[41] J. M. Luttinger, Theory of thermal transport coefficients, Phys. Rev. **135**, A1505 (1964).
[42] T. Christen and M. Büttiker, Gauge-invariant nonlinear electric transport in mesoscopic conductors, Europhys. Lett. **35**, 523 (1996).
[43] D. Sánchez and R. López, Scattering theory of nonlinear thermoelectric transport, Phys. Rev. Lett. **110**, 026804 (2013).
[44] J. Meair and P. Jacquod, Scattering theory of nonlinear thermoelectricity in quantum coherent conductors, J. Phys.: Condens. Matter **25**, 082201 (2013).
[45] C. Texier and J. Mitscherling, Nonlinear conductance in weakly disordered mesoscopic wires: Interaction and magnetic field asymmetry, Phys. Rev. B **97**, 075306 (2018).
[46] N. Dashti, M. Acciai, S. Kheradsoud, M. Misiorny, P. Samuelsson, and J. Splettstoesser, Readout of quantum screening effects using a time-dependent probe, Phys. Rev. Lett. **127**, 246802 (2021).
[47] M. V. Moskalets, *Scattering Matrix Approach to Non-stationary Quantum Transport* (World Scientific Publishing Company, London, England, 2011).
[48] P. K. Tien and J. P. Gordon, Multiphoton process observed in the interaction of microwave fields with the tunneling between superconductor films, Phys. Rev. **129**, 647 (1963).
[49] J. H. Shirley, Solution of the Schrödinger equation with a Hamiltonian periodic in time, Phys. Rev. **138**, B979 (1965).
[50] P. N. Butcher, Thermal and electrical transport formalism for electronic microstructures with many terminals, J. Phys.: Condens. Matter **2**, 4869 (1990).
[51] M. Aguilar and J. P. Paz, General theory for thermal and nonthermal quantum linear engines, Phys. Rev. A **105**, 042219 (2022).
[52] M. Aguilar and E. Lutz, Correlated quantum machines beyond the standard second law, Sci. Adv. **11**, eadw8462 (2025).
[53] R. Sánchez, J. Splettstoesser, and R. S. Whitney, Nonequilibrium system as a demon, Phys. Rev. Lett. **123**, 216801 (2019).
[54] S. E. Deghi and R. A. Bustos-Marún, Entropy current and efficiency of quantum machines driven by nonequilibrium incoherent reservoirs, Phys. Rev. B **102**, 045415 (2020).
[55] L. Tesser, R. S. Whitney, and J. Splettstoesser, Thermodynamic performance of hot-carrier solar cells: A quantum transport model, Phys. Rev. Appl. **19**, 044038 (2023).
[56] F. Battista, F. Haupt, and J. Splettstoesser, Energy and power fluctuations in ac-driven coherent conductors, Phys. Rev. B **90**, 085418 (2014).
[57] D. A. Ivanov, H. W. Lee, and L. S. Levitov, Coherent states of alternating current, Phys. Rev. B **56**, 6839 (1997).
[58] J. Keeling, I. Klich, and L. S. Levitov, Minimal excitation states of electrons in one-dimensional wires, Phys. Rev. Lett. **97**, 116403 (2006).
[59] J. Dubois, T. Jullien, F. Portier, P. Roche, A. Cavanna, Y. Jin, W. Wegscheider, P. Roulleau, and D. C. Glattli, Minimal-excitation states for electron quantum optics using levitons, Nature (London) **502**, 659 (2013).
[60] B. Bertin-Johannet, J. Rech, T. Jonckheere, B. Grémaud, L. Raymond, and T. Martin, Microscopic theory of photoassisted electronic transport in normal-metal/BCS-superconductor junctions, Phys. Rev. B **105**, 115112 (2022).
[61] E. Danielsson, H. Kirchberg, and J. Splettstoesser, Optimizing energy conversion with nonthermal resources in steady-state quantum devices, Phys. Rev. B **112**, 195434 (2025).
[62] J. Gabelli and B. Reulet, Dynamics of quantum noise in a tunnel junction under ac excitation, Phys. Rev. Lett. **100**, 026601 (2008).
[63] D. C. Glattli and P. S. Roulleau, Levitons for electron quantum optics, Phys. Status Solidi B **254**, 1600650 (2017).
[64] R. Kosloff and A. Levy, Quantum heat engines and refrigerators: Continuous devices, Annu. Rev. Phys. Chem. **65** 365 (2014).
[65] M. Moskalets and M. Büttiker, Magnetic-field symmetry of pump currents of adiabatically driven mesoscopic structures, Phys. Rev. B **72**, 035324 (2005).